Modelling and Dynamic Performance of a Direct-Drive Direct-Grid Slip Permanent Magnet Wind Generator

Pieter Bouwer, Johannes H.J. Potgieter and Maarten J. Kamper
Department of Electrical and Electronic Engineering
Stellenbosch University
Stellenbosch, South Africa
14817748@sun.ac.za, jpot@sun.ac.za, kamper@sun.ac.za

Abstract—**In this paper a transfer function model is developed to evaluate the dynamic performance of the direct-drive direct-grid connected slip permanent magnet wind generator system. The modelling of the generator is done in the *dq* reference frame fixed to the PM-rotor, for both the grid frequency and slip-frequency generator components. The transient response of a single, 15 kW grid-connected system to changes in turbine torque and grid voltage and frequency is evaluated. It is shown that the generator is very stable under transient turbine-torque conditions and that it acts as a filter to prevent voltage flickering. The dynamic performance is confirmed by laboratory measurements on a 15 kW direct drive slip permanent magnet generator.**

Keywords-direct drive; dynamic performance; grid connection; modelling; permanent magnet; wind generator.

I. INTRODUCTION

There is a trend in recent years towards the use of direct drive (gearless) permanent magnet generator (PMG) wind turbine systems [1]. These systems are connected to the grid via full-scale AC-AC power electronic solid-state converters (SSCs) as shown in Fig. 1(a) [2]. In addition to the important advantage of a gearless system, the other advantages of the converter-fed direct drive system include, among other things, variable speed maximum power point control, reactive power control and ride-through capability. With the SSC the PMG can also be operated at maximum torque per ampere or at maximum efficiency. The cost of the SSC and in general the complexity of the converter-fed PMG system can be considered as disadvantages.

Alternatively to the direct-drive converter-fed wind turbine systems, the less complex slip permanent magnet generator (S-PMG) system, recently proposed by [3], can be used. The S-PMG is a direct-drive, direct-grid connected generator system, thus, without the use of any gearbox and without any SSC as shown in Fig. 1(b). It is the simplest generator system that one can use for grid-connected wind generators, as explained in more detail in Section II. As the S-PMG system is connected directly to the grid, the wind turbine operates at a speed related to the grid frequency. Hence, the utility-grid-connected S-PMG system operates basically at fixed speed, which makes maximum power point operation at different wind speeds impossible. However, the S-PMG can also be connected to a variable-voltage variable-frequency converter-fed grid as shown in Fig. 1(c). This option is investigated by [4] using S-PMGs in a HVDC grid-connected wind farm. In this case the speed of the S-PMG can be varied by varying the grid frequency, by which maximum power point operation for all wind conditions can be obtained.

The question, however, of the proposed S-PMG system is the stability of the generator under transient turbine torque and transient grid voltage conditions. In the work presented in this paper, there is an attempt to answer this question by evaluating the dynamic performance of the grid-connected S-PMG system. The *dq* modelling of this special generator and the transfer function model of the whole system, receive specific attention. The investigation is done only on a small-scale wind turbine power level (sub 100 kW) by presenting detailed analysis and measurements of a 15 kW S-PMG wind energy system.

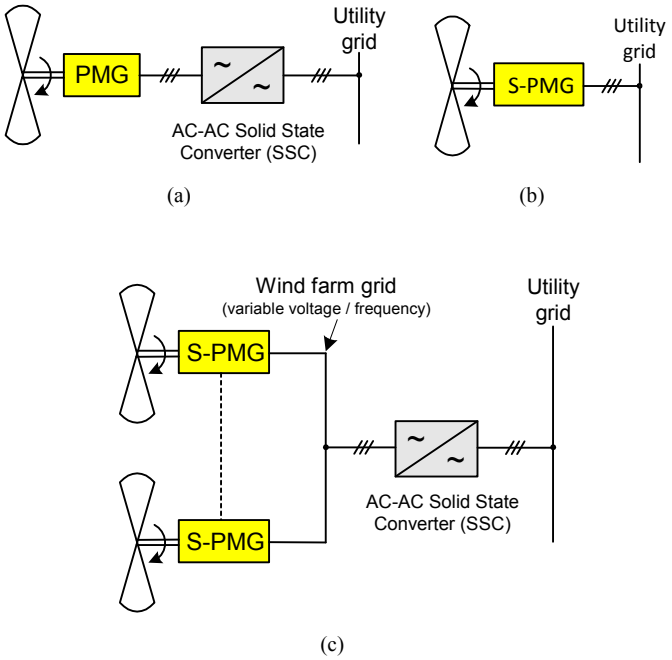

Figure. 1. Diagrams of (a) converter-fed PMG, (b) direct-grid S-PMG and (c) variable voltage/frequency wind-farm-grid S-PMG wind energy system.

The research presented in this paper was funded by the National Research Foundation (NRF) in South Africa.

II. DESCRIPTION OF THE S-PMG

The S-PMG consists of two PM generator components that are connected with each other via a free rotating PM-rotor as shown in Fig. 2. A 3D CAD drawing of the real S-PMG wind generator is shown in Fig. 3.

The one generator of the S-PMG is a synchronous generator (SG) of which the stationary stator is connected to the grid. The PM-rotor operates at synchronous speed with respect to the stator of the SG. The other generator, called the induction generator (IG), consists of a short-circuited slip rotor that is mechanically connected to the turbine. The slip rotor operates at slip speed with respect to the PM-rotor. A torque, T_r, is generated between the slip rotor and the PM-rotor, while a counter torque, T_s, is generated between the stator and the PM-rotor. Power transfer, thus, takes place from the turbine to the slip rotor, and then via the PM-rotor to the stator and the grid.

It must be noted that the proposed S-PMG in Figs. 2 and 3 is completely different from the conventional PM induction generator, as investigated e.g. by [5 – 7].

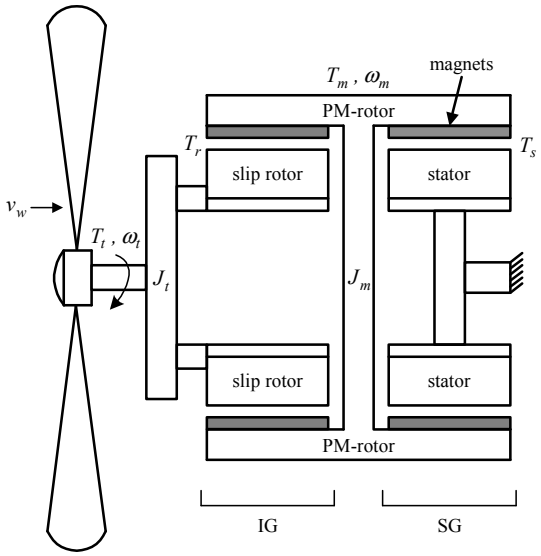

Figure 2. Concept diagram of the S-PMG.

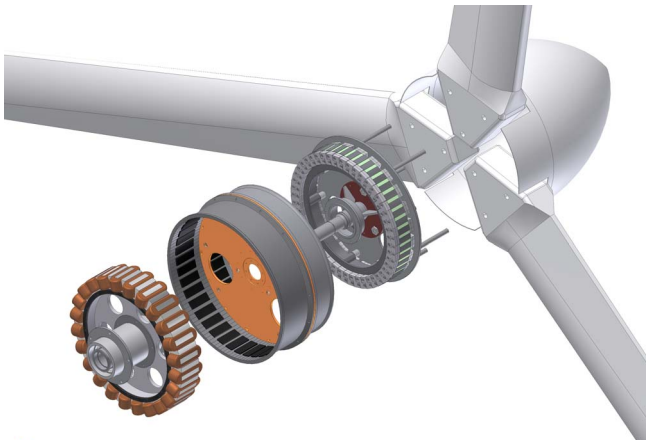

Figure 3. CAD drawing of the S-PMG connected to the wind turbine (stator left, PM-rotor middle and slip-rotor right [3].

III. MODELLING OF THE S-PMG

From Fig. 2 it is clear that the S-PMG can be modelled as two separate, decoupled machines as shown in the per phase equivalent circuit of Fig. 4. In this circuit, the rotor is referred to the grid frequency. As can be seen the rotor winding is short-circuited and mechanically connected to the turbine, while the stator winding is connected to the grid. In the case of the stator a voltage is induced at grid frequency in the steady state, while in the case of the short-circuited rotor a voltage is induced at slip frequency. The slip speed is taken as positive in generator mode. Positive power transfer, thus, is from the turbine to the IG, and then via the SG to the grid.

The *dq* equivalent circuits of the IG and SG are shown in Fig. 5. Note that positive current is taken as flowing out of the machine. Hence, the *dq* dynamic equations of the IG and the SG fixed to the PM-rotor are given respectively by

$$\begin{aligned} 0 &= -i_{qr}R_r - L_{qr}\frac{di_{qr}}{dt} - \omega_{sle}L_{dr}i_{dr} + \omega_{sle}\lambda_{mr} \\ 0 &= -i_{dr}R_r - L_{dr}\frac{di_{dr}}{dt} + \omega_{sle}L_{qr}i_{qr} \end{aligned} \tag{1}$$

and

$$\begin{aligned} v_{qs} &= -i_{qs}R_s - L_{qs}\frac{di_{qs}}{dt} - \omega_{me}L_{ds}i_{ds} + \omega_{me}\lambda_{ms} \\ v_{ds} &= -i_{ds}R_s - L_{ds}\frac{di_{ds}}{dt} + \omega_{me}L_{qs}I_{qs} \end{aligned} \tag{2}$$

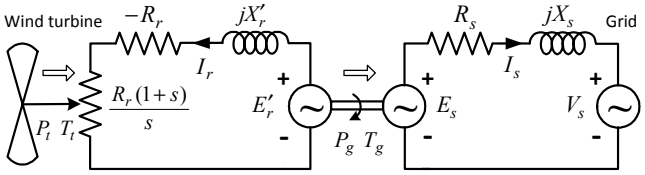

Figure. 4. Steady-state per phase equivalent circuit of the S-PMG.

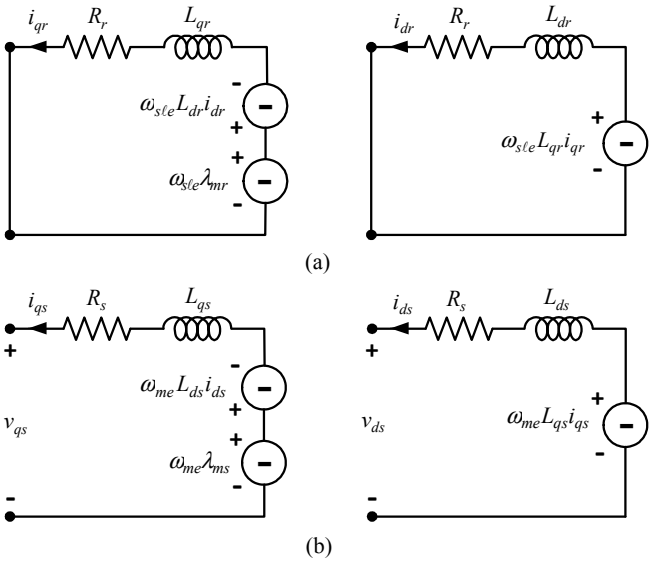

Figure 5. *dq* equivalent circuits of (a) short-circuited slip rotor and (b) stator of the S-PMG.

where ω_{sle} is the electrical slip speed equal to $\omega_{sle} = (\omega_t - \omega_m)p/2$, and where ω_t and ω_m are the turbine and PM-rotor angular velocities respectively (see Fig. 2) and p the number of poles, and where $\omega_{me} = \omega_m\, p/2$. Further in (1) and (2), subscript "r" indicates IG-rotor and "s" indicates SG-stator. Hence, (L_{qr} , L_{dr}) and (L_{qs} , L_{ds}) in (1) and (2) are the dq inductances of respectively the IG-rotor and SG-stator, and λ_{mr} and λ_{ms} are respectively the IG and SG flux linkages due to the permanent magnets.

The torques generated by the IG and SG as indicated in Fig. 2 are given respectively by

$$T_r = \tfrac{3}{4}\, p[(L_{qr} - L_{dr})i_{dr}i_{qr} + \lambda_{mr}i_{qr}] \qquad (3)$$

and

$$T_s = \tfrac{3}{4}\, p[(L_{qs} - L_{ds})i_{ds}i_{qs} + \lambda_{ms}i_{qs}]\,. \qquad (4)$$

The dynamics of the turbine (plus slip rotor) and PM-rotor are expressed by (5) and (6) as

$$T_t - T_r = J_t \frac{d\omega_t}{dt} \qquad (5)$$

and

$$T_m = T_r - T_s = J_m \frac{d\omega_m}{dt}\,, \qquad (6)$$

where T_t is the torque generated by the turbine and T_m the resultant torque acting on the PM-rotor, and where J_t and J_m are respectively the inertias of the turbine (plus slip rotor) and PM-rotor as shown in Fig. 2.

For accurate simulation, the PM flux linkages, λ_{mr} and λ_{ms}, and the saturated dq inductances are obtained from static finite element (FE) solutions of the IG and SG. The cross-sections of the IG and SG generators used in the FE analysis are shown in Fig. 6. For the IG a non-overlapping distributed double layer cage winding is used as shown in Fig. 6(a). For the SG a non-overlapping concentrated single layer winding is used as shown in Fig. 6(b); the choice of a single layer winding is mainly due to cost reasons as explained by [3] and [8]. Both the IG and SG have 40 poles and 48 slots, resulting in a 10-12 pole-slot combination for both.

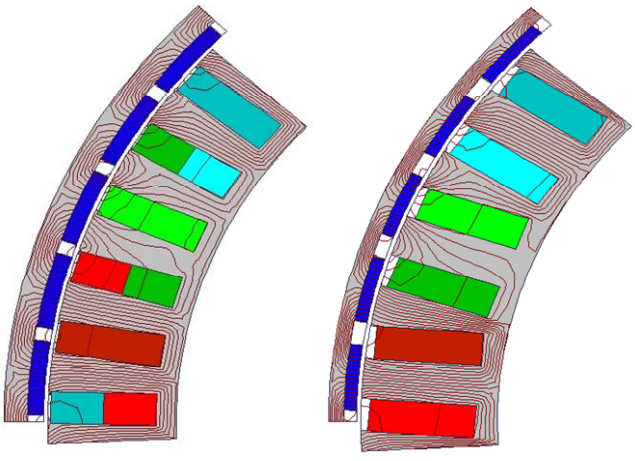

(a) (b)

Figure 6. Cross sections and FE plots of (a) double layer cage IG rotor and (b) single layer SG stator of the S-PMG (rated per phase rms values of the circuit in Fig. 4 are: I_r = 6.5 kA, I_s = 23 A, V_s = 400 V).

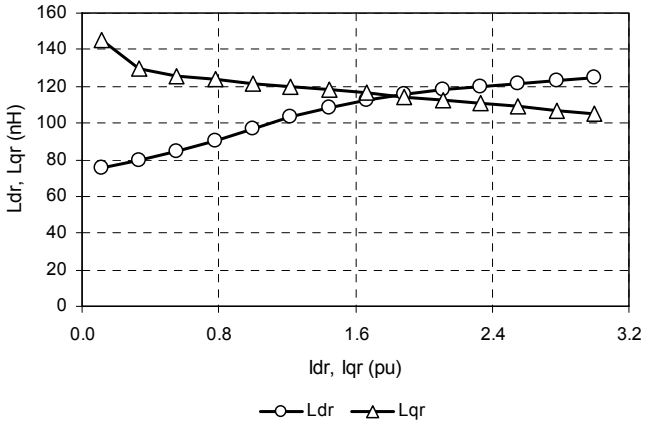

Figure 7. L_{dr} (I_{qr}=0) and L_{qr} (I_{dr}=0) inductances versus I_{dr} and I_{qr} of the IG cage slip rotor (rated rotor bar current is I_{dr} = 2.7 kA; I_{qr} = 8.8 kA).

The dq inductances of the IG and SG circuits of Fig. 5 are determined in general by

$$L_q = \frac{\lambda_q}{-i_q}\,; \qquad L_d = \frac{\lambda_d - \lambda_m}{-i_d}\,. \qquad (7)$$

The dq inductances of (7) are affected by saturation and cross-coupling effects. The dq inductances, for example, of the IG cage rotor of Fig. 6(a) are shown in Fig. 7. It is shown that L_{dr} increases with I_{dr}, because the flux is weakened and there is thus less magnetic saturation. In turn, L_{qr} reduces with I_{qr} due to higher magnetic saturation. Note that the PM flux linkage λ_m in (7) also varies slightly with load. However, to keep the modelling and simulation simple in this first investigation, constant (rated) values for the dq inductances and PM flux linkages are assumed in (1) and (2).

IV. Simulation Results

From the mathematical model in the previous section a complete transfer function simulation model of a single grid-connected S-PMG wind energy system is obtained as shown in Fig. 8. This simulation is implemented in Matlab Simulink. The model is also written in VHDL to be used in the SIMPLORER simulation package. The Function Generator (FG) in Fig. 8 gives the torque-speed curves of the turbine with the wind speed, v_w, as an input parameter. The voltages v_{abc} are the per phase grid voltages that are transformed to v_{dqs} of (2). The rest of the simulation diagram is self explanatory from the equations in Section III.

The response of the S-PMG system to transient turbine torque and transient grid voltage conditions are investigated in the following sections using the developed simulation model in Fig. 8. The inertias and electrical parameters used in the simulation of the S-PMG wind turbine of Figs. 2 and 3, are summarized in Table I.

TABLE I. Simulation Parameters

J_t = 300 kg.m^2	R_r = 3.84 μΩ	L_{dr} = 100 nH	L_{ds} = 7.5 mH
J_m = 5 kg.m^2	R_s = 0.4 Ω	L_{qr} = 120 nH	L_{qs} = 10 mH
p = 40	f_s = 50 Hz	λ_{mr} = 3.69 mWb.t	λ_{ms} = 1.04 Wb.t

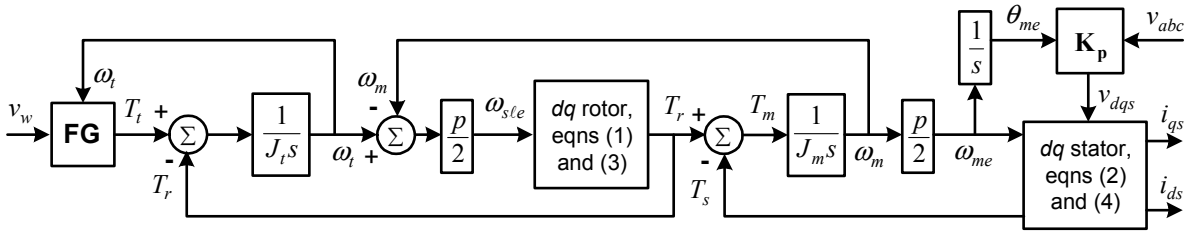

Figure. 8. Transfer function diagram of the grid-connected S-PMG wind energy system ($\mathbf{K_p}$ is Park's transformation).

A. Transient Turbine Torque Conditions

The transient response of the S-PMG system for a 10 m/s step input in wind speed (equivalent to a step input in turbine torque) is shown in Fig. 9. The SG's torque in Fig. 9(a) and SG's line current in Fig. 9(b) show a very stable over-damped step response.

The frequency response of the generator system is furthermore investigated, with the result shown in Fig. 10. This shows that the 15 kW S-PMG wind turbine system has a bandwidth of about 1 Hz. Tower shadow and yaw error will generate a turbine torque pulsation frequency of 7.5 Hz for the investigated fixed speed S-PMG system; this is calculated at a no-load turbine speed of 150 r/min with the S-PMG connected to a 50 Hz grid. This frequency (7.5 Hz) is well above the system's cut-off frequency of 1 Hz, and, hence, explains the zero torque-output response in Fig. 11 to a 7.5 Hz turbine-torque-frequency input. This is a significant result for the proposed fixed speed S-PMG wind turbine system, as possible voltage flickering on the grid due to tower shadowing and yaw error [9] will not occur.

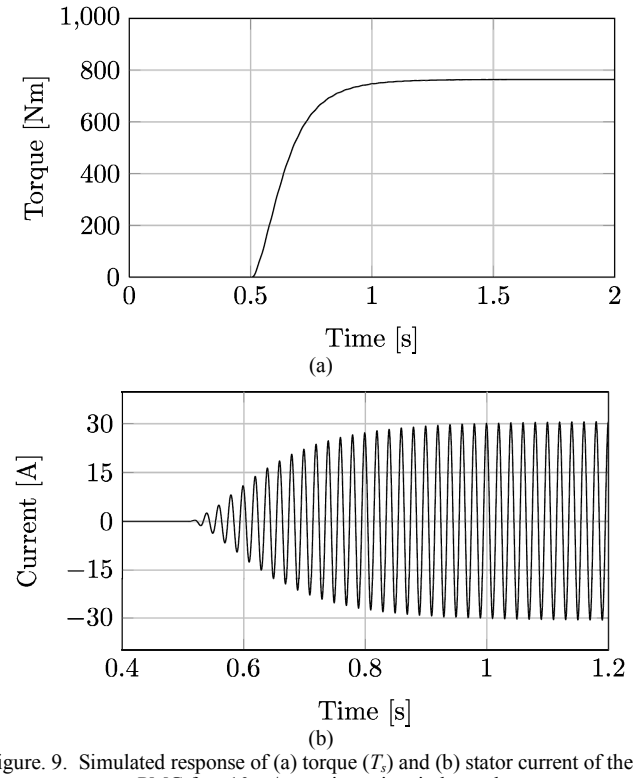

Figure. 9. Simulated response of (a) torque (T_s) and (b) stator current of the S-PMG for a10 m/s step input in wind speed.

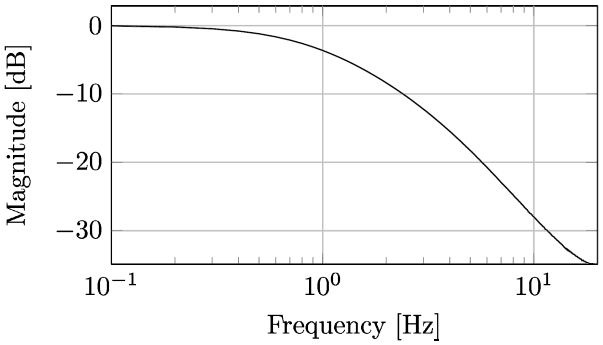

Figure. 10. Frequency response of T_s / T_t of the S-PMG system.

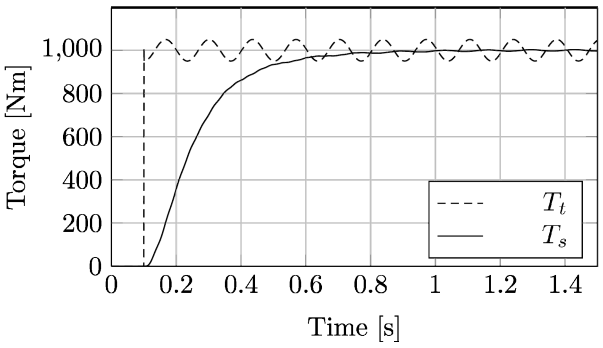

Figure. 11. Simulated torque (T_s) response of the S-PMG for a step + 7.5 Hz turbine torque (T_t) input.

B. Transient Grid Voltage Conditions

The effect of transient and harmonic grid voltages on the stability of the S-PMG system are as import to investigate. In Fig. 12 with the S-PMG at full-load (1000 Nm and 23 A rms), the effect of a 20 % step drop in the grid voltage on the SG's torque and *dq* currents are shown. From this it is clear that the SG of the S-PMG is quite sensitive to grid voltage changes, but that the SG also stabilises relatively fast (within 50 ms) from the worst transients. What is interesting, though, is that the speed of the free-rotating PM-rotor, ω_m, is also affected by this condition as shown in Fig. 12(a). This can be explained by the relatively small inertia, J_m, of the PM-rotor in Fig. 8 that acts little as a filter against high frequency torques (in this case a 50 Hz torque component). This is an important observation as the IG operation is then affected by this condition due to the feedback speed (ω_m) in Fig. 8. Finally, shown by the *dq* currents in Fig. 12(b) in the steady state, the S-PMG compensates for low (in this case) or high grid voltages by supplying (in this case) or drawing reactive power to or from the grid respectively.

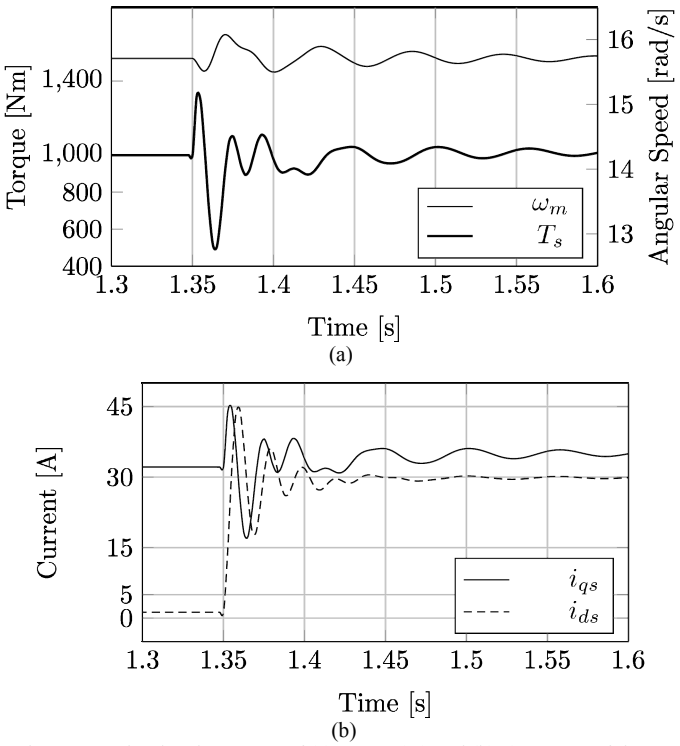

Figure. 12. Simulated response of (a) torque (T_s) and (b) *dq* current of the S-PMG for a 20 % step-drop in grid voltage.

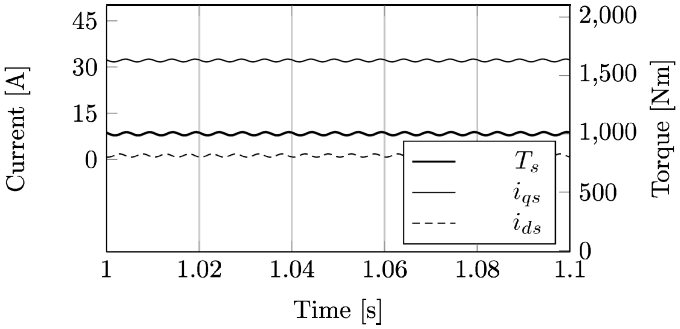

Figure. 13. Simulated *dq* current and torque of the SG with a 2 % 5th-harmonic voltage in the grid voltage.

To study the effect of harmonic grid voltages, a 2 % 5th-harmonic voltage is added to the v_{abc} grid voltage in the simulation in Fig. 8. The effect of this on the SG's torque and current with the S-PMG under full-load, is shown in Fig. 13. It is clear that the 5th-harmonic voltage causes a 5th harmonic *dq* stator current to flow and a (5-1)f_s-frequency (200 Hz in this case) generated torque. This high frequency torque has little effect on the speed, ω_m, of the PM-rotor due to its inertia J_m (Fig. 8), and, thus, has little effect on the IG operation.

V. Measured Results

The 15 kW S-PMG of Fig.3 has been built and tested in the laboratory. Due to time constraints, however, and due to the fact that the proposed double layer IG cage rotor of Fig. 6(a) is very expensive to build, the IG slip rotor is wound with a non-overlapping double layer winding. This changed the inductance and resistance parameter values of Table I to: L_{dr} = 4.6 mH, L_{qr} = 7.9 mH and R_r = 0.33 Ω. The test system with the S-PMG is shown in Fig. 14. An induction motor plus gearbox drive system is used to drive the S-PMG. The induction motor drive was put under torque control (not speed control) to simulate turbine torque transients.

With the S-PMG connected to a 400 V, 50 Hz grid, a step input torque of 1000 Nm is given to the motor drive system. The measured response of the input shaft torque and stator current of the S-PMG is shown in Fig. 15. The simulated current response using the measured shaft torque as torque input in the simulations, is shown in Fig. 16. From these figures the agreement between measured and simulated current responses is clear. The low frequency oscillation in the amplitude of the measured current is caused by the torque ripple of the IG's slip rotor.

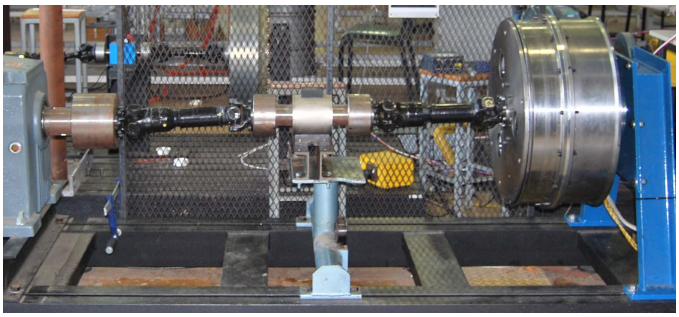

Figure. 14. Test system with the induction drive motor + gear box (left) connected to the S-PMG (right) via a torque sensor.

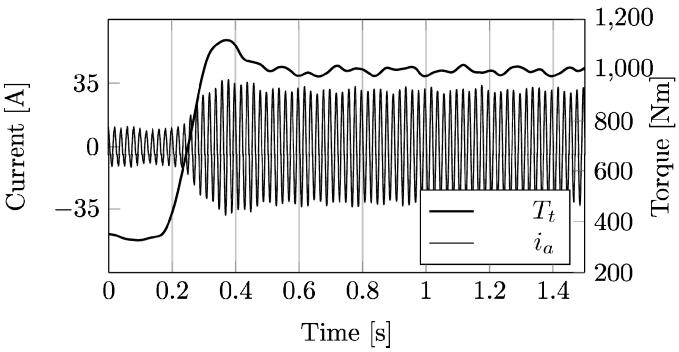

Figure. 15. Measured shaft torque (T_t) and current response of the S-PMG system for a step input torque command given to the drive motor system.

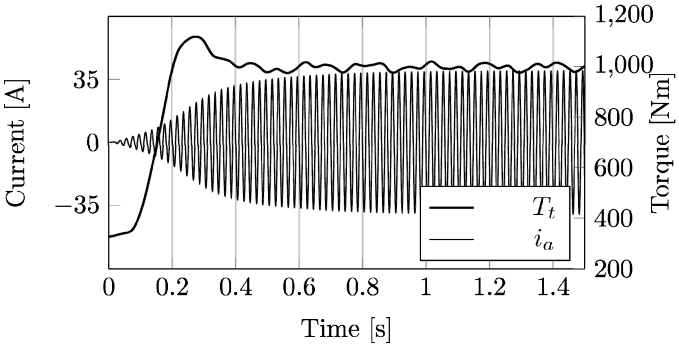

Figure. 16. Simulated current response of the S-PMG system with the same torque input as measured in Fig. 15.

Grid voltage transients could not be simulated in the laboratory at time of submission of the paper. Therefore, no measured results of the effect of transient grid voltages on the S-PMG system could be presented.

VI. CONCLUSIONS

In this paper a transfer function model is developed for the direct-drive, direct-grid connected slip permanent magnet wind generator (S-PMG) system. From the simulated and measured response of a 15 kW S-PMG system it is shown that the system is very stable under transient turbine torque conditions. In particular it is found that the S-PMG wind generator system has a very low bandwidth. This causes the system to act as a filter against turbine pulsation torques caused by e.g. tower shadow and jaw error, which prevent voltage flickering from occuring.

It is furthermore shown that the S-PMG is sensitive to grid voltage changes, which affects, amongst other things, its ride-through capability. Grid harmonic voltages are shown to cause harmonic currents of the same order to flow in the S-PMG. The amplitudes of these harmonic currents depend on the internal impedance of the SG. In this regard the SG with a single layer non-overlapping winding has the advantage of a higher internal impedance, and, thus, lower harmonic currents that flows. Finally, transient grid voltages (not harmonic voltages) at the terminals of the SG are shown in the paper have an effect on the IG operation of the S-PMG system.

REFERENCES

[1] A.D. Hansen and L.H. Hansen, "Market penetration of wind turbine concepts over the recent years", Proc. European Wind Energy Conference and Exhibition 2007, Milan (Italy), May 2007.

[2] H. Li and Z. Chen, "Overview of different wind generator systems and their comparisons", IET Renewable Power Generation, vol. 2, 2008, pp. 123-138.

[3] J.H.J. Potgieter and M.J. Kamper, "Design of new concept permanent magnet induction wind generator", IEEE Energy Conversion Congress & Expo (ECCE), Atlanta (USA), 12-16 Sept. 2010.

[4] R. Vermaak, J.H.J. Potgieter and M.J. Kamper, "Grid-Connected VSC-HVDC Wind Farm System and Control Using Permanent Magnet Induction Generators", IEEE International Conference on Power Electronics and Drive Systems (PEDS), Tapei, Taiwan, Nov. 2009.

[5] W.F. Low, N. Schofield, "Design of a permanent magnet excited induction generator", Proc. of the International Conference on Electrical Machines (ICEM), Manchester (United Kingdom), 1992, vol. 3, pp. 1077-1081.

[6] B. Hagenkort, T. Hartkopf, A. Binder and S. Jockel, "Modelling a direct drive permanent magnet induction machine", Proc. of the International Conference on Electrical Machines (ICEM), Espoo (Finland), Aug. 2000, pp. 1495-1499.

[7] G. Gail, T. Hartkopf, E. Troster, M. Hoffling, M. Henschel and H.Schneider, "Static and dynamic measurements of a permanent magnet induction generator: test results of a new wind generator concept", Proc. of the International Conference on Electrical Machines (ICEM), Cracow (Poland), Sept. 2004.

[8] J.H.J. Potgieter and M.J. Kamper, "Cogging torque sensitivity in design optimisation of low cost non-overlap winding PM wind generator", Proc. of the International Conference on Electrical Machines (ICEM), Rome (Italy), Sept. 2010.

[9] Det Norske Veritas (DNV) and Riso National Laboratory, Guidelines for Design of Wind Turbines, 2nd ed., printed by Scanprint a/s Denmark, 2009.